AGU PUBLICATIONS

Space Weather

FEATURE ARTICLE
10.1002/2017SW001726

Key Points:
- Real-time data from Van Allen Probes are valuable for space weather operations
- Particle changes at geostationary orbit can be easily monitored from Van Allen Probes space weather data
- Simultaneous Van Allen Probes and NOAA-GOES data can provide improved space environment information to geostationary satellite operators

Correspondence to:
J. Lee,
jjlee@kasi.re.kr

Citation:
Lee, J., Kim, K.-C., Giuseppe, R., Ukhorskiy, S., Sibeck, D., Kessel, R., … Lee, J. (2018). Space weather operation at KASI with Van Allen Probes beacon signals. *Space Weather*, *16*, 108–120. https://doi.org/10.1002/2017SW001726

Received 16 SEP 2017
Accepted 19 JAN 2018
Accepted article online 25 JAN 2018
Published online 7 FEB 2018

Space Weather Operation at KASI With Van Allen Probes Beacon Signals

Jongkil Lee[1,2], Kyung-Chan Kim[3], Romeo Giuseppe[4], Sasha Ukhorskiy[4], David Sibeck[5], Ramona Kessel[6], Barry Mauk[4], Barbara Giles[5], Bon-Jun Gu[7], Hyesook Lee[8], Young-Deuk Park[1], and Jaejin Lee[1,2]

[1]Korea Astronomy and Space Science Institute, Daejeon, South Korea, [2]University of Science and Technology, Daejeon, South Korea, [3]Division of Science Education, College of Education, Daegu University, Gyeongsan, South Korea, [4]Applied Physics Laboratory, The Johns Hopkins University, Laurel, MD, USA, [5]NASA Goddard Space Flight Center, Greenbelt, MD, USA, [6]NASA Headquarters, Washington, DC, USA, [7]Electronics and Telecommunications Research Institute, Daejeon, South Korea, [8]National Meteorological Satellite Centre, Korea Meteorological Administration, Jincheon-gun, South Korea

Abstract The Van Allen Probes (VAPs) are the only modern National Aeronautics and Space Administration (NASA) spacecraft broadcasting real-time data on the Earth's radiation belts for space weather operations. Since 2012, the Korea Astronomy and Space Science Institute (KASI) has contributed to the receipt of these data via a 7 m satellite-tracking antenna and used these beacon data for space weather operations. An approximately 15 min period is required from measurement to acquisition of Level-1 data. In this paper, we demonstrate the use of VAP data for monitoring space weather conditions at geostationary orbit (GEO) by highlighting the Saint Patrick's Day storm of 2015. During that storm, Probe-A observed a significant increase in the relativistic electron flux at 3 R_E. Those electrons diffused outward resulting in a large increase of the electron flux >2 MeV at GEO, which potentially threatened satellite operations. Based on this study, we conclude that the combination of VAP data and National Oceanic and Atmospheric Administration-Geostationary Operational Environmental Satellite (NOAA-GOES) data can provide improved space environment information to geostationary satellite operators. In addition, the findings obtained indicate that more data-receiving sites would be necessary and data connections improved if this or a similar system were to be used as an operational data service.

1. Introduction

As modern society is increasingly technologically dependent, space weather monitoring and forecasting are also growing in importance (Baker, Kanekal, et al., 2004; Jonas & McCarron, 2015; Lanzerotti, 2004; Svalgaard, 2013). National Aeronautics and Space Administration (NASA)'s twin Van Allen Probe (VAP) spacecraft broadcast space weather data from an orbit covering altitudes ranging from 600 to 30,000 km within the region containing the radiation belts (Baker et al., 2013). A radiation belt is a torus of energetic charged particles trapped in the Earth's magnetic field (Friedel et al., 2002). The Earth's ring current, which results in geomagnetic storms when intensified, manifests in the same region (Chen et al., 2006; Ukhorskiy et al., 2010). Therefore, in the context of space weather, the VAPs are constantly monitoring some of the most important regions in space (Morley et al., 2010; Reeves, 2007).

The presence of high-energy charged particles in the Earth's radiation belts is thought to be one of the main causes of performance degradation in solar panels, temporary problems with telecommunication and positioning systems, and malfunctions of onboard satellite computing systems (Choi et al., 2011; Horne et al., 2013; Lohmeyer et al., 2015; Lanzerotti & Baker, 2017; Wrenn, 1995). Rapid solar wind changes influence current systems in the magnetosphere that in turn alter the magnetic field at the Earth's surface and disturb the ionosphere, sometimes causing communication disturbances, power grid interruptions, and Global Positioning System errors (Aarons, 1991; Spogli et al., 2009). According to data from the Combined Radiation Release and Effects Satellite, the Solar Anomalous and Magnetospheric Particle Explorer, Polar, and Time History of Events and Macroscale Interactions during Substorms missions, the plasma environment in the inner magnetosphere experiences extremely dynamic changes within only a few hours (Baker, Daly, et al., 2004; Blake et al., 1992; Green & Kivelson, 2004; Hwang et al., 2013; Li et al., 2001; Reeves et al., 1998). The rapid changes have been difficult to monitor in real time, however. Because the focus of these missions is scientific and the data were not available in near real time, these spacecraft could not be used for space weather forecasts and alerts.

Figure 1. Satellite tracking antenna constructed at KASI for receipt of VAP space weather data.

In contrast, when building the VAPs NASA included the provision to broadcast space weather data in near real time, again demonstrating the value of applying a satellite intended for scientific observation missions to space weather operations as was done with the Advanced Composition Explorer (ACE) mission (Kirby & Stratton, 2013; Zanetti et al., 2014). The probes launched on 30 August 2012 orbit Earth once every 9 h and broadcast space weather data to Earth over a 21.5 h period, excluding the 2.5 h when they broadcast the full scientific data set (Kessel et al., 2013). Currently, four countries—South Korea, the Czech Republic, Brazil, and Argentina—routinely receive space weather data from the VAPs. Further, the Johns Hopkins University Applied Physics Laboratory (JHU/APL) provides Level-1 data products to space weather customers. In 2011, the Korea Astronomy and Space Science Institute (KASI) concluded a letter of agreement for science cooperation with NASA. Subsequently, KASI constructed a satellite receiver antenna with a diameter of 7 m (Figure 1), with which it has been receiving data from the probes for space weather monitoring. It is the efforts of KASI that is the subject of this report.

To protect the safety of its geostationary orbit (GEO) satellites, KASI uses data from the Geostationary Operational Environmental Satellite (GOES) system, provided by the National Oceanic and Atmospheric Administration (NOAA), to discern the space environment around the satellites. The NOAA-GOES satellites

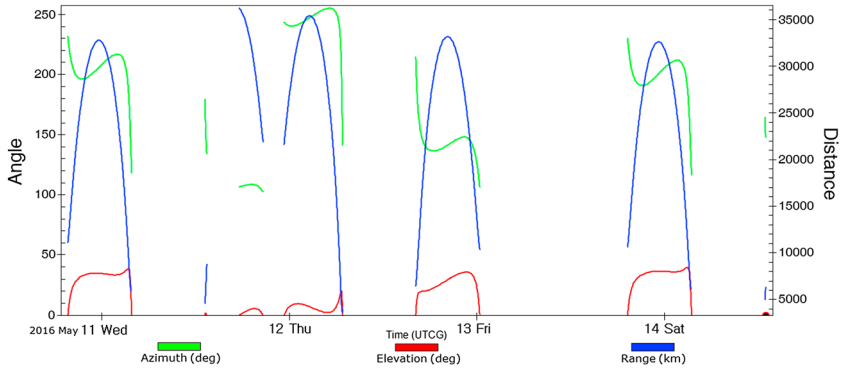

Figure 2. Antenna angles for tracking VAP-A. When the elevation angle (shown in red) is greater than 10°, the antenna targets the VAP spacecraft to receive space weather data.

monitor conditions at GEO, and the data are delivered quickly to space weather forecasters. Based on the past 5 years of monitoring with the VAPs, this report concludes that more effective, three-dimensional monitoring of the space environment can be achieved by combining the NOAA-GOES data with the VAP space weather beacon observations. Further, assimilative models, such as the Dynamic Radiation Environment Assimilation Model (Reeves et al., 2012), Salammbô (Bourdarie & Maget, 2012), and the Versatile Electron Radiation Belt (Subbotin & Shprits, 2009) codes for space weather prediction are more effectively run with multiple data sources.

This report demonstrates the knowledge gained through use of VAP near-real-time beacon data for space weather operations, which has the potential to aid the design and operation of future space weather missions targeting a similar orbit. We discuss the receipt and processing methods for the space weather data, along with the usage of these data for space weather monitoring at KASI. In addition, we examine changes in the space environment at GEO using the VAP data.

2. Receipt of Near-Real-Time Space Weather Data From the VAPs

Figure 1 shows the satellite-tracking antenna installed at KASI that was designed to receive the appropriate S-band satellite signals. The antenna targets the satellite location according to predetermined orbit information. Figure 2 plots the directional changes of the antenna required to receive data from satellite-A. KASI has determined that tracking one probe is sufficient and is optimal for efficient antenna operation. The satellites have an inclination angle of 10.2°; in Daejeon, South Korea, where the KASI antenna is installed (latitude: 36.4°, longitude: 127.4°), the elevation angle is less than 45°. Thus, the antenna tracks the spacecraft without data loss when the elevation angle is sufficiently large (more than 10°). Figure 2 shows a time span of 4 days, three of which featured optimum conditions for data reception when the satellite remained at a relatively high elevation angle (greater than 30°) for individual periods of approximately 6.5 h. The elevation angle was occasionally less than 10° or remained above 10° only a short time, as for the contact interval on 12 May (Figure 2). In such cases, data loss occurs. Generally, in South Korea, the antenna receives space weather data approximately 20% of the time. The data are transmitted to the ground via S-band using 8 W solid-state power amplifier transmitters (Kirby et al., 2013).

Figure 3 illustrates the method by which the real-time data are received and processed. At KASI, raw data are received directly from the probes via the local antenna. The data are stored in a recording device within KASI and simultaneously sent to JHU/APL in real time. To ensure security, these data are encrypted through secure shell tunneling between KASI and JHU/APL. At JHU/APL, the raw data are automatically converted to Level-1 data in the space weather data server, which removes unactionable data and reorganizes the packets in time order. Real-time processing of the most current data, that is, that received within the previous 24 h, is performed every 10 min. A separate process runs twice daily to reprocess the telemetry of the previous 2 days. Multithreading, in parallel, intakes the data from each instrument. Most of the code written in Perl, Interactive Data Language, and C is in-house software, whereas some code has been provided by instrument teams (e.g., Energetic Particle Composition and Thermal Plasma Suite (ECT)). Newly created common data format (CDF)

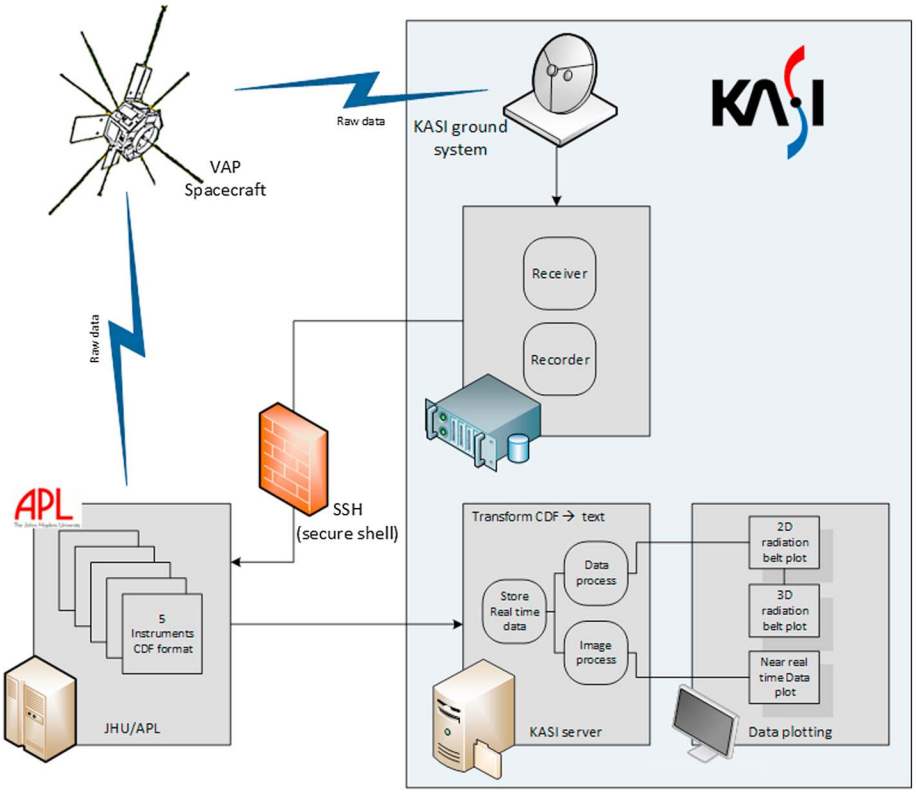

Figure 3. Diagram showing data flow from VAPs to JHU/APL. Near-real-time space weather data are converted to Level-1 data and distributed to the global space weather community.

files are delivered to external sites and made available to the public via the Radiation Belt Storm Probes (RBSP) Science Gateway (http://rbspgway.jhuapl.edu/). A period of approximately 15 min is required for the following process: The VAPs observe the environmental conditions and send the data to JHU/APL; JHU/APL preprocesses the data and sends them in the form of Level-1 data in a CDF file to users. At KASI, Level-1 files in CDF format are converted into text files, which are used as basic data for near-real-time monitoring of the space environment. As the CDF format constitutes compressed text data, a small file size is obtained; thus, programs such as Autoplot (http://autoplot.org) can be used for easy visual representation of the data. However, for practical handling of observations from the VAPs for the purposes of space weather operations, data in text format are deemed more useful than that in CDF file format, at least at KASI.

During the process of converting a CDF file into a text file, error values have been removed and the information of satellite location is added as may be necessary. For example, for Magnetic Electron Ion Spectrometer (MagEIS) data, the CDF file contains timestamps and particle data and does not contain satellite location data. Therefore, Electric and Magnetic Field Instrument and Integrated Science (EMFISIS) data, which do contain satellite location data, are referenced and matched with MagEIS data based on timestamps. In addition, the data sometimes contain consecutive identical values or nonphysical values; these duplicate or outlier values are eliminated, and the data are rearranged to allow real-time display based on the current satellite location.

Figure 4a shows the space weather data volume received from VAP-A from the period January 2013 (when KASI first began receiving VAP data) to May 2017. As the data volume over the course of 1 day (the right *y* axis) is proportional to the time at which the space weather data are received (the left *y* axis), the *y* axes can be used to indicate both data volume and time (see Figure 4a). The satellite receiver antenna operated by KASI maintains contact with the satellite for more than 6.5 h at a time; however, the contact period can span more than 1 day and so the data plotted in units of days may appear uneven. Because daily changes in reception status apply to all four VAP receiving stations (in South Korea, the Czech Republic, Brazil, and

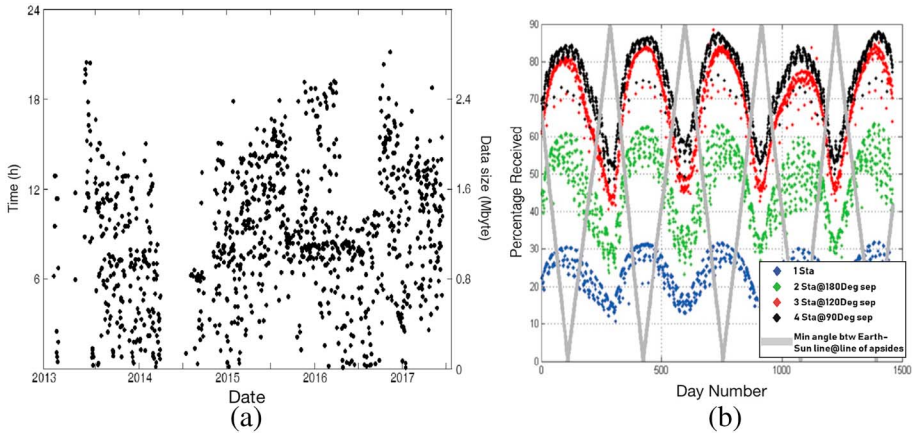

Figure 4. (a) Daily sizes of VAP-A space weather data from January 2013 to May 2016. The daily size depends on the time coverage for the space weather data. (b) Expected average contact time per day (%) between VAP spacecraft and one or more ground stations distributed worldwide, plus minimum angle between Earth-Sun line and line of apsides (deg) shown in Kessel et al. (2013).

Argentina), the scatter plot presents data volume in units of days, as shown in Figure 4a. In addition, as data loss occasionally occurs, and as unactionable data are eliminated during the Level-1 data conversion process, the data volume converted to Level-1 data varies daily. Further, because the VAPs do not transmit space weather data for 2.5 h of every 24 h period (in order to send science data), the maximum duration for which space weather data can be received is 21.5 h. Overall, up to 85% of the total data can be received at the four different sites; thus, the maximum reception duration has been calculated to be 18.2 h (Kessel et al., 2013). Note that the maximum reception time shown in Figure 4a has a similar value.

The two radio frequency antenna beams from the VAPs are aligned with the spacecraft spin and antispin axes perpendicular to the plane of the solar panel pointing toward the Sun. When the spacecraft-Earth line is perpendicular to the Sun-Earth line (parallel to the spin axis), the antenna patterns are not appropriately aligned with the Earth, which means that the space weather data cannot be received on the Earth's surface during those times (Kessel et al., 2013). Thus, the reception ratio was expected to vary from 80% to 50% over a period of approximately 300 days, as shown in Figure 4b (Stratton et al., 2013). However, Figure 4a does not show this variation in reception ratio. It seems that, contrary to expectations, the radio waves remain sufficiently strong that beacon signals can be received even when the beam is almost perpendicular to the Earth. The approximately 100 days worth of data missing from March 2014 onward was due to a problem with the network system. Effective links with the data processing systems between KASI and JHU/APL are an important component of our space weather operations, especially with regard to the utilization of the space weather data.

3. Application of VAP Space Weather Data

Space weather plots created by KASI can be viewed on the following website: http://sos.kasi.re.kr/center/monitor_rbsp.php. Figure 5 shows an example of the space weather display showing data obtained by VAP-A. Data from 2 days previously, 1 day previously, and the present day are shown in purple, blue, and red, respectively. While JHU/APL provides real-time space weather plots with a time sequence (http://rbspgway.jhuapl.edu/rPlotTime?sw), KASI adds to that set with intuitive plots that depict the data with respect to distance from the Earth. Space weather forecasters can easily identify the current space environment. The KASI website also provides the means to download the equivalent text format data via the file transfer protocol.

The VAPs are equipped with five different investigations that facilitate more than 20 types of space weather observation, including data on electrons, ions, electric and magnetic fields, and the spacecraft electric potential. A detailed description of the data is available in Kessel et al. (2013). The 12 types of data thought to be particularly relevant for space weather monitoring are shown in Figure 5, with the corresponding details listed in Table 1. While the clear connections between space environment and satellite malfunction have not

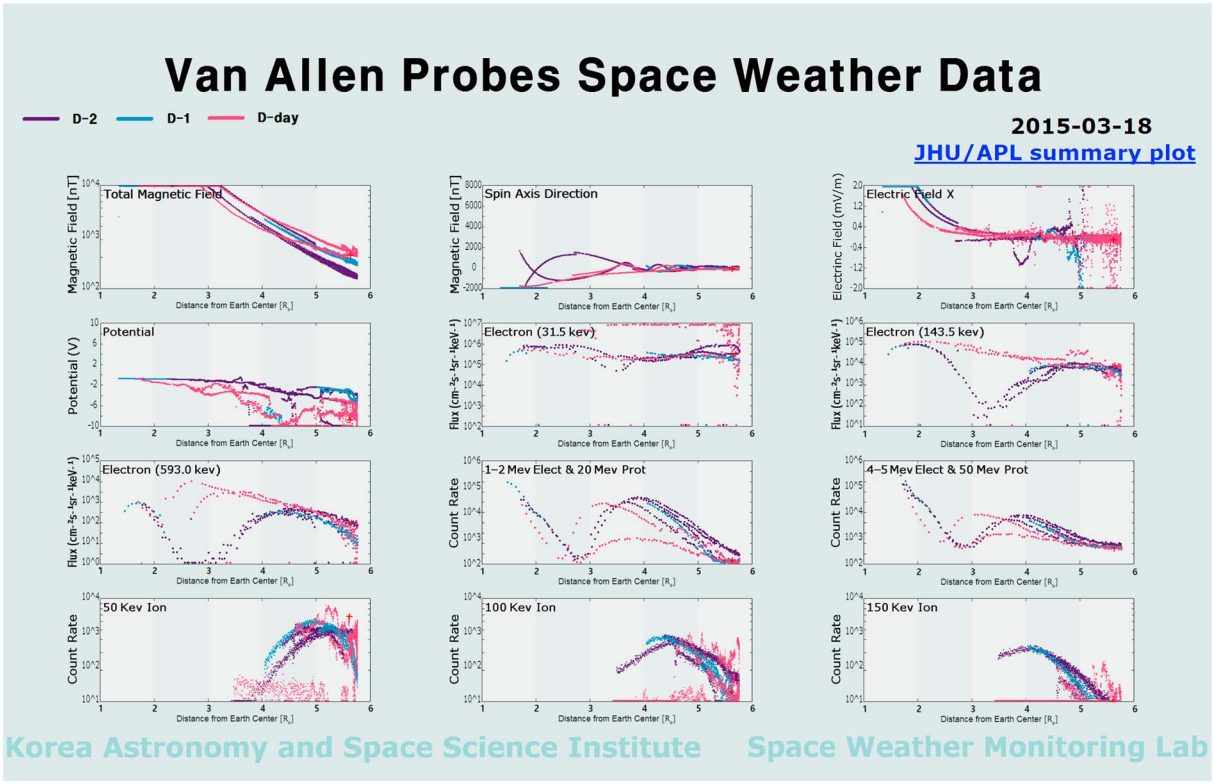

Figure 5. Sample VAP space weather data display from 18 March 2015. These panels show some of the VAP data versus distance from the Earth's surface (*x* axis) for the previous 3 days. The red, blue, and purple lines display VAP data on the present day, 1 day previously, and 2 days previously, respectively.

revealed, statistical analysis implies that the internal/external spacecraft charging caused by wide energy particles could be the main source of satellite anomalies (Baker et al., 1987; Fennell et al., 2000; Sarno-Smith et al., 2016; Thomsen et al., 2013). A recent study reports GEO satellites experience the more hostile space weather conditions in the midnight to dawn section after geomagnetic storms (Choi et al., 2011) and support the connection between spacecraft charging and anomalies.

The VAPs have a spin stabilization attitude control system, and the time variation of the real-time rotational-direction magnetic field data renders recognition of geomagnetic field disturbance difficult. Thus, we display total and spin-axis-direction magnetic field data in Figure 5. The changes of the geomagnetic field due to

Table 1
Details of VAP Space Weather Data Types Shown in Figure 5

Space weather data	Instrument	Description
Total magnetic field	EMFISIS/Magnetometer (MAG)	Magnitude of three-vector magnetic field
Spin axis magnetic field	EMFISIS/MAG	Satellite spin-axis-directional magnetic field
Potential	Electric Field and Waves (EFW)	Spacecraft potential measured by EFW
Electron (32.7 keV)	ECT/MagEIS	26–40 keV Electron flux
Electron (129 keV)	ECT/MagEIS	113–145 keV Electron flux
Electron (580 keV)	ECT/MagEIS	514–646 keV Electron flux
Electron (1,040 keV)	ECT/MagEIS	969–1121 keV Electron flux
Electron and proton	ECT/Relativistic Electron Proton Telescope (REPT)	Count rate: 1−2 MeV electrons and >20 MeV protons
Electron and proton	ECT/REPT	Count rate: 4−5 MeV electrons and >50 MeV protons
Ion (50 keV)	Radiation Belt Storm Probes Ion Composition Experiment (RBSPICE)	Energetic proton count rate
Ion (100 keV)	RBSPICE	Energetic proton count rate
Ion (150 keV)	RBSPICE	Energetic proton count rate

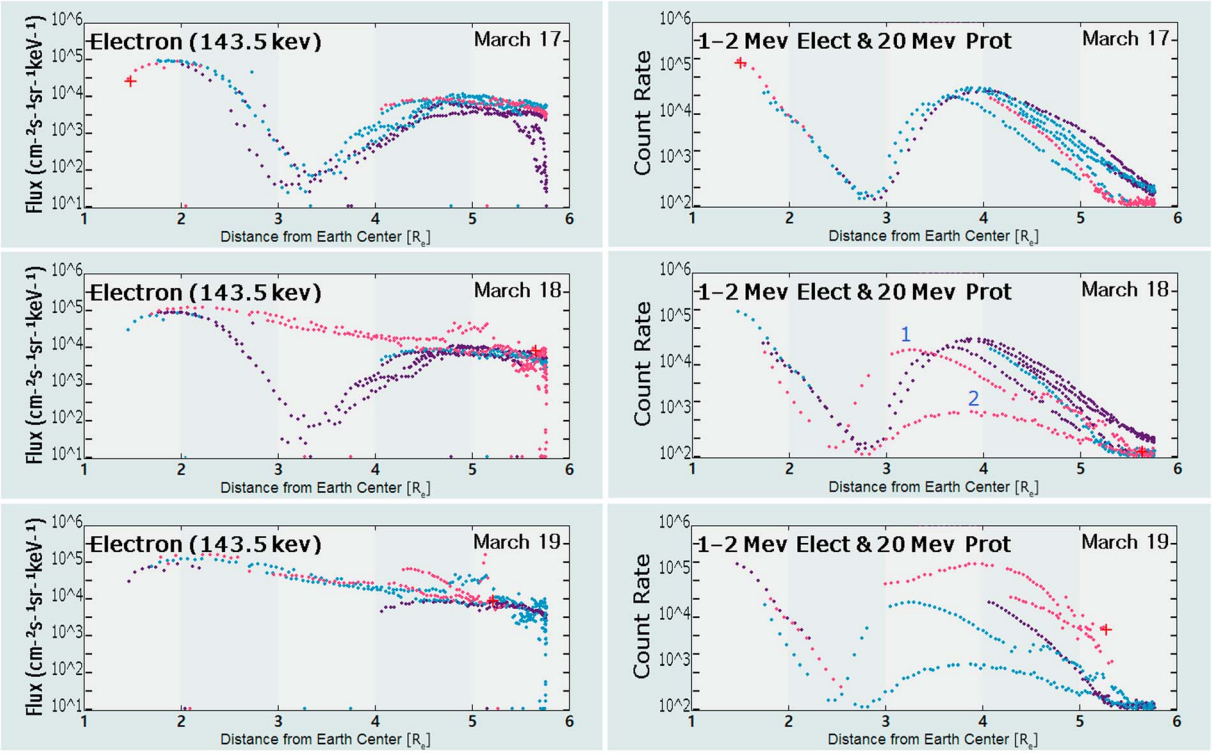

Figure 6. Radiation belt particle variation caused by Saint Patrick Day's Storm on 17 March 2015. The red, blue, and purple lines display the VAP data on the present day, 1 day previously, and 2 days previously, respectively.

solar wind variation appear more clearly at the apogee point than near the Earth. Because the orbit and attitude of the satellite do not change considerably over a 3 day period, examination of the magnetic field data measured over 3 days is an effective indicator of the degree of disturbance in the current magnetic field. Because the field near the Earth does not uniform, it is apparent that the magnetic field data in the spin-axis-direction varies greatly each orbit. Note the spacecraft potential varies greatly during a geomagnetic storm. We also monitor electron and ion fluxes over a broad energy range as an important space weather factor. In this study, we chose six energy ranges for the electrons: 31.5, 143.5, and 593 keV and 1, 1−2, and 4−5 MeV and three energy ranges for the ions: 50, 100, and 150 keV. These particle data also show dramatic changes during the storm under study; however, it has not yet been possible to determine which energies are most effective for monitoring space weather risks. Further study is necessary to identify the connection between these inner magnetosphere space weather factors and apparent spacecraft malfunctions.

Figure 6 shows an example of the dramatic changes in the Earth's radiation belts during a storm that are evident in the VAP space weather beacon data. On 15 March 2015, at 02:00 UT, a coronal mass ejection (CME) from the Sun was observed. Solar wind data from the Advanced Composition Explorer (ACE) satellite indicate that the CME reached the vicinity of the Earth approximately 2 days later, on 17 March at 03:00 UT. Just as the CME reached the Earth, there was a disruption in the planet's magnetic field, causing the Kp index to increase significantly to a value of 8 at approximately 12:00 UT. This disruption in the Earth's magnetic field lasted until 19 March and is referred to as the "Saint Patrick's Day Storm." This event and its consequences have been studied extensively, because it is the strongest in Solar Cycle 24 (Astafyeva et al., 2015; Kamide & Kusano, 2015; Morley et al., 2016; Pierrard & Lopez Rosson, 2016). In this study, the primary focus is on the viability of using real-time data from within the radiation belts to gain actionable space weather nowcasting and forecasting information during a strong geomagnetic storm.

On 17 March, a relatively small volume of near-real-time space weather observation data was received compared to other days (indicated in red in the top row of Figure 6). This day has a similar profile as the previous day. There was an increase in the electron flux (143.5 keV) at 2−4.5 R_E on 18 March. The 1−2 MeV electron flux throughout the entire outer region of the radiation belt showed dramatic changes in the two orbits passing

through. In the first pass on 18 March, labeled "1" in Figure 6, VAP-A observed an electron flux decrease for which only 2% of the maximum electron flux at 3.5 R_E remained, with the rest being relocated elsewhere. This was likely due to the Dst effect combined with magnetopause shadowing, which can move electrons outward and cause electron loss through the magnetopause (Kim et al., 2010). In addition, other nonadiabatic processes such as outward radial diffusion (Shprits et al., 2006) and precipitation into the atmosphere by wave-particle interaction (Horne et al., 2009; Kremser et al., 1986; Thorne & Kennel, 1971) can act as major loss processes. The probable loss mechanism is beyond the scope of this study; however, the study does demonstrate that with VAP space weather beacon observations, rapid global-scale electron loss processes in the radiation belt can be effectively monitored.

In the next pass (labeled "2" in Figure 6), which occurred approximately 5 h later, a significant increase in electron flux was observed at approximately 3.2 R_E. For electron fluxes with low-energy levels (143.5 keV), the distributions remained at a high level for the entire 3 day duration in near geosynchronous orbit (>5 R_E). For electron fluxes with energies greater than 1 MeV, the distributions decreased and then increased on 18 and 19 March. A possible reason for this behavior is that the inflow electrons may have been accelerated by a wave-particle interaction associated with whistler mode chorus waves, by a factor of 31 or greater compared to the time at which the storm occurred (Horne et al., 2005; Li et al., 2014; Summers et al., 2007; Thorne et al., 2013). This hypothesis has been confirmed using VAP science observations, which indicated strong chorus waves in the 3.5 R_E region.

While the one-dimensional graphs shown in Figures 5 and 6 are effective for professional forecasters that monitor space weather, space weather data should also be displayed so that information is effectively conveyed to space weather end users. Accordingly, we developed software displaying VAP data in a three-dimensional space (Figure 7). The VAP orbit is generally close to Earth's magnetic equator, and only the flux of particles distributed near the Earth's equator is observed. However, charged particles bounce along the Earth's magnetic field, having been caught in the field; thus, particle distributions at other latitudes can also be determined from the flux in the Earth's equatorial plane. The particle flux can be reasonably calculated for a three-dimensional space. When the particle distribution (j_0) within the Earth's equatorial plane is given, the omnidirectional particle fluxes (J_λ) distributed along the line of magnetic force can be estimated by integrating over the equatorial pitch angles (α_0) that can reach the magnetic latitude λ, following Hess (1968). Thus,

$$J_\lambda = 4\pi \frac{B_\lambda}{B_0} \int_0^{\sin^{-1}\left(\sqrt{B_0/B_\lambda}\right)} j_0(\alpha_0) \frac{\sqrt{\left(1 - \sin^2\alpha_0\right)}}{\sqrt{1 - \left(B_\lambda/B_0\right)\sin^2\alpha_0}} \sin\alpha_0 \mathrm{d}\alpha_0,$$

where B_0 and B_λ are the field intensities at the equator and λ, respectively. The Tsyganenko T02 model is used to obtain the magnetic field values (Tsyganenko, 2002).

When creating three-dimensional particle flux plots, we assume that the equatorial particle flux has a pitch angle distribution corresponding to a sine function peaking at 90°. In addition, we impose the assumption that the VAP particle data do not differ significantly from the equatorial flux, while the probes sample an approximately 40° (±20°) range of magnetic latitudes (Morley et al., 2016). These two assumptions potentially yield errors in the high-latitude region; however, this visualization tool is developed for users such as satellite operators rather than being for scientific research. As a proof of concept and initial deployment of useful, actionable space weather products, these errors are considered insignificant and the focus is on the intuitive representation of space weather information for users.

Figure 7 shows a representation of near-real-time data (1,040 keV electrons) from VAP-A in a three-dimensional space mapped onto the Tsyganenko magnetic field. With a simple mouse operation, users can switch between the side (Figure 7 top) and top (Figure 7 bottom) views. An animation showing the changes in the radiation belts over the past 2 days ago is also available. Using our system, users can quickly, and perhaps automatically, determine the extent to which a geostationary satellite may be affected by changes in the radiation belts. The location of Korean GEO satellites, NOAA-GOES, and the VAPs are displayed on the radiation belt map. Users can easily customize the map and add the location of other operational satellites. The 3-D visualization tool is available for space weather users under the condition of noncommercial use. The software will be provided as an execution file operating on Windows system; it currently assumes

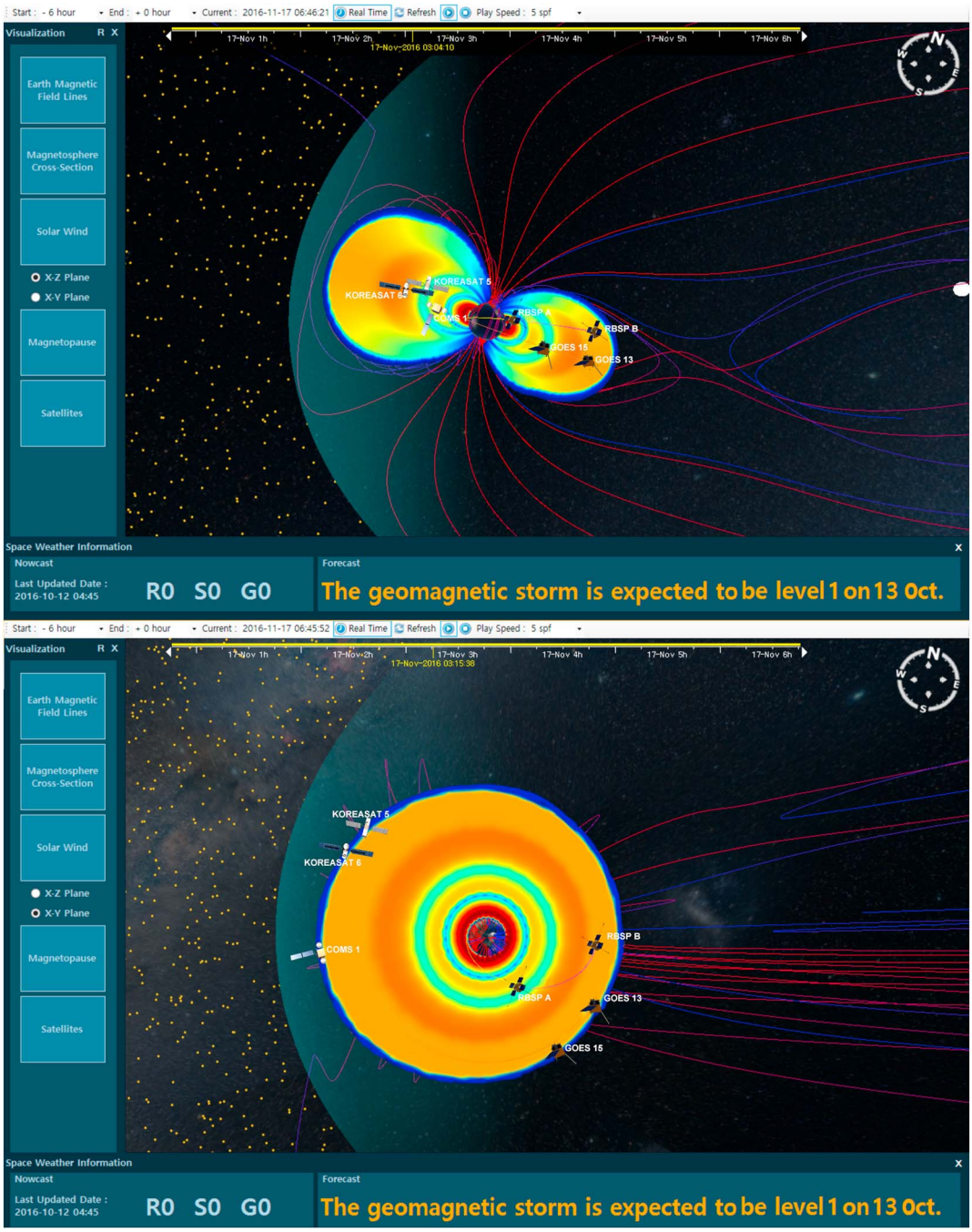

Figure 7. Three-dimensional visualization of VAP space weather data for 1−2 MeV electrons. With simple mouse movements, the radiation belt view direction can be changed.

that the user's computer is connected to KASI's data server on the Internet to download the current space weather data in the appropriate formats.

4. Comparison of VAPs and NOAA-GOES Data

Figure 8 plots the location of each satellite (GOES-13 and VAP-A), projected on the equatorial plane with 1 h intervals (indicated by circle), for 16–20 March, the period when the Saint Patrick's Day event occurred. VAP-A is in a geotransfer orbit, with a period of about 9 h, while GOES-13 is in a GEO, with a period of 24 h. Because

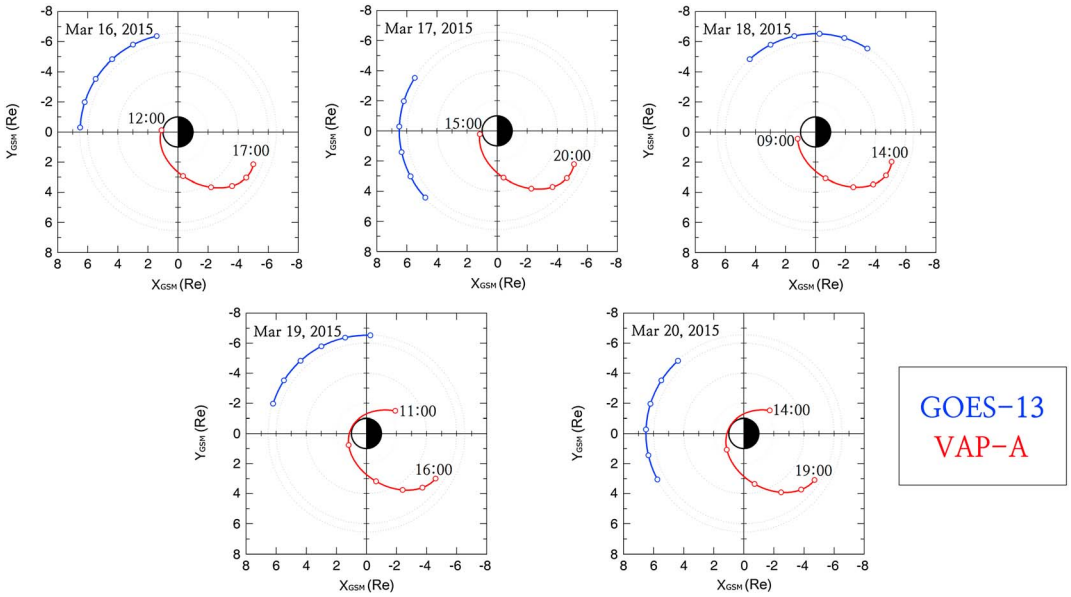

Figure 8. Spacecraft positions at 1 h intervals (GOES-13 (blue) and VAP-A (red)).

the apogee of VAP-A is ~30,000 km in a near-equatorial elliptical orbit, particle distributions at geostationary satellites that orbit Earth, such as GOES-13 (36,000 km), can be estimated by combining the extrapolation method and past geostationary satellite particle data.

Figure 9 compares space weather data from VAP-A and GOES-13 (> 2 MeV electrons) during the Saint Patrick's Day event. The VAP-A data are differential flux data where the electron flux was measured for each of the energy levels, while the GOES-13 data are integral flux data where the electron flux data were integrated up to a reference energy level. Near-real-time MagEIS data from VAP-A were used to align the observation energy bands of the two satellites. Electron energy spectra from six MagEIS energy channels ranging from 31.5 to 1077 keV were fit to an exponential function. Integral fluxes were calculated from the resulting function by integrating data points with energy levels greater than 2 MeV. VAP-A data are shown with circles, while GOES-13 data are shown with squares where the error bars show the standard deviation of the NOAA-GOES data for the period of VAP measurements on each day. The fluxes for different days are color coded.

On 17 March, GOES-13 measured an electron flux near 12.0 (/cm^2/s/sr). After 1 day (18 March), this flux had increased by 79 times, and after 2 days (19 March), it had increased by 1,203 times. Examination of the data

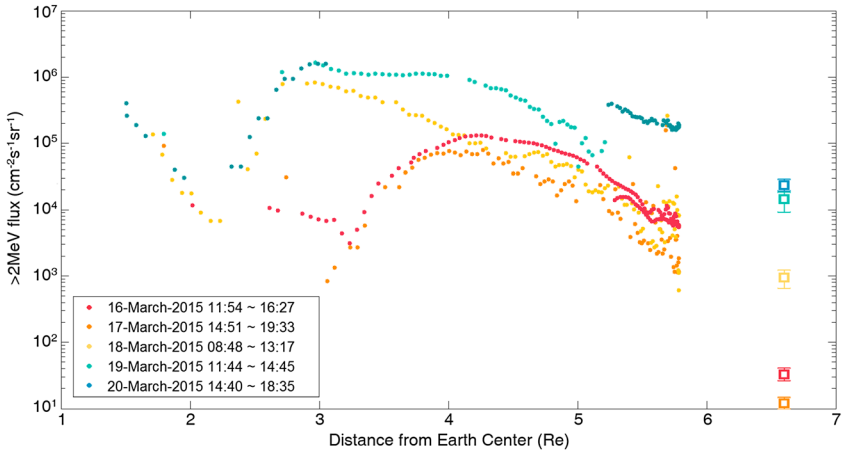

Figure 9. VAP-A and GOES-13 beacon data for Saint Patrick Day's event.

from 16 to 17 March indicates that the flux decreased slightly before beginning to rise rapidly on 18 March. Note that, if we were to consider the GEO data (GOES $>$ 2 Mev) alone, it would be difficult to infer exactly what had occurred.

Meanwhile, the electron flux observed by VAP-A decreased overall at all locations on 17 March relative to 16 March. Further, note that the decrease was greater with greater distance from the Earth. As a result, the electron flux at GOES-13 decreased on 16 March relative to 17 March. This reduction in electron flux may have resulted from loss due to electron precipitation, or it may have been due to relativistic electron dropout caused by a magnetopause shadowing effect. In addition, it may have been caused by an adiabatic response to the changing magnetic field during the storm period (Kim & Chan, 1997). A detailed discussion of the drivers behind this electron loss is beyond the scope of this paper.

On 18 March, the Saint Patrick's Day event was in its recovery phase. On that day, VAP-A observed a rapid increase in the number of electrons with energies greater than 2 MeV, in the region between 2.5 and 3.5 R_E. Furthermore, on 19 and 20 March, VAP-A observed that the electron flux was gradually increasing in the exterior region of the radiation belts. This can be interpreted as electron motion from the interior to the exterior of the radiation belts due to outward radial diffusion from the newly accelerated populations by wave-particle interactions. GOES-13 also recorded an increase in electron flux starting from 18 March. If the rapid increase in electron flux in the interior of the radiation belt on 18 March had not been discovered, it would have been difficult to predict the changes in electron flux at GEO after 18 March. By observing the electron flux in the interior of the radiation belts, however, changes in particle distribution in the GEO can easily be inferred. Therefore, it is our conclusion that space weather data—similar to that available from the VAPs—are important for predicting particle changes at GEO.

5. Conclusions

This study has demonstrated the feasibility of using VAP beacon data for space weather operations. When a space weather event occurs, space weather users in Korea receive radio blackout (R), solar radiation storm (S), and geomagnetic storm (G) information scaled by NOAA through a social network service or through the broader media. In many cases, the users contact space weather forecasters to query predictions regarding the related behavior in space. Before the VAP satellites were launched, only limited near-real-time information on the structure of the radiation belts could be obtained from space. KASI does not run a model predicting particle flux in GEO orbit with VAP data; however, forecasters include information of the near-real-time radiation belt variation in the text message that is delivered to the satellite operators.

A period of approximately 15 min is required from the time of observation at the spacecraft to generation and distribution of the final space weather data. Using these space weather data, the current status of the radiation belts can be promptly determined. On its website, KASI displays 12 different plots featuring VAP space weather data as a function of distance from the Earth. By combining VAP and NOAA-GOES magnetic field data, the radiation and magnetic field changes in the Earth's magnetosphere can be easily understood. This information is useful for satellite operators, for example, by those controlling satellite attitude with a magnetic torquer. Further, the spacecraft potential can indirectly indicate low-energy plasma condition around the satellite. Above all, because particle fluxes at GEO are affected by the radiation belts inside these orbits, particle changes at the GEO can be forecast from particle changes measured by the VAPs.

The VAPs are the first satellites to provide near-real-time information specifically from the Earth's radiation belts. Typically, data from the NOAA-GOES geostationary satellites are used to aid in the monitoring of changes in the radiation belts. As these spacecraft observe electron fluxes from a fixed radial distance, they have limited applicability for detecting changes in the radiation belts and for providing space weather data to users. The analysis of the Saint Patrick's Day event based on VAP and NOAA-GOES data has shown that relativistic electrons of the radiation belts are first accelerated in the 3−4 R_E region and that electron fluxes then increase at GEO. In this study only one event is discussed; however, many such events have been recorded in the operational VAP space weather data. Many previous studies have concluded that electrons are accelerated at distance of 3−4 R_E and then diffuse outward to GEO (Baker et al., 1998; Jaynes et al., 2015; Miyoshi et al., 2003). The findings of this study indicate that simultaneous use of VAP space weather data and NOAA-GOES data provides space weather forecasters with significantly more useful information on the space environment than with previous techniques.

Acknowledgments
The authors thank the reviewers for their detailed and insightful comments, which have improved this paper. This work was supported by the National Meteorological Satellite Centre (NMSC) of the Korea Meteorological Administration (KMA), through the "Geostationary Meteorological Satellite Ground Segment Development" research project. In accordance with AGU data policy, we inform readers that Van Allen Probe space weather data are available at http://rbspgway.jhuapl.edu/ and http://sos.kasi.re.kr/center/monitor_rbsp.php. NOAA-GOES satellite particle data are available at http://www.ngdc.noaa.gov/stp/satellite/goes/dataaccess.html. The three-dimensional image shown in Figure is an electron distribution snapshot generated by customized software. We provide this software for free under a noncommercial use agreement. Readers who wish to obtain this software should email a request to jjlee@kasi.re.kr.

References

Aarons, J. (1991). The role of the ring current in the generation or inhibition of equatorial *F* layer irregularities during magnetic storms. *Radio Science*, *26*(4), 1131–1149. https://doi.org/10.1029/91RS00473

Astafyeva, E., Zakharenkova, I., & Förster, M. (2015). Ionospheric response to the 2015 St. Patrick's Day storm: A global multi-instrumental overview. *Journal of Geophysical Research: Space Physics*, *120*, 9023–9037. https://doi.org/10.1002/2015JA021629

Baker, D. N., Belian, R. D., Higbie, P. R., Klebesadel, R. W., & Blake, J. B. (1987). Deep dielectric charging effects due to high-energy electrons in Earth's outer magnetosphere. *Journal of Electrostatics*, *20*(1), 3–19. https://doi.org/10.1016/0304-3886(87)90082-9

Baker, D. N., Daly, E., Daglis, I., Kappenman, J. G., & Panasyuk, M. (2004). Effects of space weather on technology infrastructure. *Space Weather*, *2*, S02004. https://doi.org/10.1029/2003SW000044

Baker, D. N., Hoxie, V. C., Jaynes, A., Kale, A., Kanekal, S. G., Li, X., … Spence, H. E. (2013). James Van Allen and his namesake NASA mission. *Eos Transactions - American Geophysical Union*, *94*(49), 469–470. https://doi.org/10.1002/2013EO490001

Baker, D. N., Kanekal, S. G., Li, X., Monk, S. P., Goldstein, J., & Burch, J. L. (2004). An extreme distortion of the Van Allen belt arising from the Halloween solar storm in 2003. *Nature*, *432*(7019), 878–881. https://doi.org/10.1038/nature03116

Baker, D. N., Li, X., Blake, J. B., & Kanekal, S. (1998). Strong electron acceleration in the Earth's magnetosphere. *Advances in Space Research*, *21*(4), 609–613. https://doi.org/10.1016/S0273-1177(97)00970-8

Blake, J. B., Kolasinski, W. A., Fillius, R. W., & Mullen, E. G. (1992). Injection of electrons and protons with energies of tens of MeV into $L < 3$ on 24 March 1991. *Geophysical Research Letters*, *19*(8), 821–824. https://doi.org/10.1029/92GL00624

Bourdarie, S. A., & Maget, V. F. (2012). Electron radiation belt data assimilation with an ensemble Kalman filter relying on the Salammbô code. *Annales de Geophysique*, *30*(6), 929–943. https://doi.org/10.5194/angeo-30-929-2012

Chen, Y., Friedel, R. H. W., & Reeves, G. D. (2006). Phase space density distributions of energetic electrons in the outer radiation belt during two Geospace Environment Modeling Inner Magnetosphere/Storms selected storms. *Journal of Geophysical Research*, *111*, A11S04. https://doi.org/10.1029/2006JA011703

Choi, H.-S., Lee, J., Cho, K.-S., Kwak, Y.-S., Cho, I.-H., Park, Y.-D., … Lee, D.-K. (2011). Analysis of GEO spacecraft anomalies: Space weather relationships. *Space Weather*, *9*, S06001. https://doi.org/10.1029/2010SW000597

Fennell, J. F., Koons, H. C., Chen, M. W., & Blake, J. B. (2000). Internal charging: A preliminary environmental specification for satellites. *IEEE Transactions on Plasma Science*, *28*(6), 2029–2036. https://doi.org/10.1109/27.902230

Friedel, R. H. W., Reeves, G. D., & Obara, T. (2002). Relativistic electron dynamics in the inner magnetosphere—A review. *Journal of Atmospheric and Solar - Terrestrial Physics*, *64*(2), 265–282. https://doi.org/10.1016/S1364-6826(01)00088-8

Green, J. C., & Kivelson, M. G. (2004). Relativistic electrons in the outer radiation belt: Differentiating between acceleration mechanisms. *Journal of Geophysical Research*, *109*, A03213. https://doi.org/10.1029/2003JA010153

Hess, W. N. (1968). *The radiation belt and magnetosphere*. Waltham, MA: Blaisdell Co.

Horne, R. B., Glauert, S. A., Meredith, N. P., Boscher, D., Maget, V., Heynderickx, D., & Pitchford, D. (2013). Space weather impacts on satellites and forecasting the Earth's electron radiation belts with SPACECAST. *Space Weather*, *11*, 169–186. https://doi.org/10.1002/swe.20023

Horne, R. B., Lam, M. M., & Green, J. C. (2009). Energetic electron precipitation from the outer radiation belt during geomagnetic storms. *Geophysical Research Letters*, *36*, L19104. https://doi.org/10.1029/2009GL040236

Horne, R. B., Thorne, R. M., Glauert, S. A., Albert, J. M., Meredith, N. P., & Anderson, R. R. (2005). Timescale for radiation belt electron acceleration by whistler mode chorus waves. *Journal of Geophysical Research*, *110*, A03225. https://doi.org/10.1029/2004JA010811

Hwang, J., Lee, D.-Y., Kim, K.-C., Shin, D.-K., Kim, J.-H., Cho, J.-H., … Turner, D. L. (2013). Significant loss of energetic electrons at the heart of the outer radiation belt during weak magnetic storms. *Journal of Geophysical Research: Space Physics*, *118*, 4221–4236. https://doi.org/10.1002/jgra.50410

Jaynes, A. N., Baker, D. N., Singer, H. J., Rodriguez, J. V., Loto'aniu, T. M., Ali, A. F., … Reeves, G. D. (2015). Source and seed populations for relativistic electrons: Their roles in radiation belt changes. *Journal of Geophysical Research: Space Physics*, *120*, 7240–7254. https://doi.org/10.1002/2015JA021234

Jonas, S., & McCarron, E. D. (2015). Recent US policy developments addressing the effects of geomagnetically induced currents. *Space Weather*, *13*, 730–733. https://doi.org/10.1002/2015SW001310

Kamide, Y., & Kusano, K. (2015). No major solar flares but the largest geomagnetic storm in the present solar cycle. *Space Weather*, *13*, 365–367. https://doi.org/10.1002/2015SW001213

Kessel, R. L., Fox, N. J., & Weiss, M. (2013). The Radiation Belt Storm Probes (RBSP) and space weather. *Space Science Reviews*, *179*(1-4), 531–543. https://doi.org/10.1007/s11214-012-9953-6

Kim, H.-J., & Chan, A. A. (1997). Fully adiabatic changes in storm time relativistic electron fluxes. *Journal of Geophysical Research*, *102*(A10), 22,107–22,116. https://doi.org/10.1029/97JA01814

Kim, K. C., Lee, D.-Y., Kim, H.-J., Lee, E. S., & Choi, C. R. (2010). Numerical estimates of drift loss and Dst effect for outer radiation belt relativistic electrons with arbitrary pitch angle. *Journal of Geophysical Research*, *115*, A03208. https://doi.org/10.1029/2009JA014523

Kirby, K., Artis, D., Bushman, S., Butler, M., Conde, R., Cooper, S., … Williams, B. (2013). Radiation Belt Storm Probes—Observatory and environments. *Space Science Reviews*, *179*(1-4), 59–125. https://doi.org/10.1007/s11214-012-9949-2

Kirby K., & Stratton, J. (2013). Van Allen Probes: Successful launch campaign and early operations exploring Earth's radiation belts. In *Proceedings of the 2013 IEEE Aerospace Conference*.

Kremser, G., Korth, A., Ullaland, S., Stadsnes, J., Baumjohann, W., Block, L., … Amata, E. (1986). Energetic electron precipitation during a magnetospheric substorm and its relationship to wave particle interaction. *Journal of Geophysical Research*, *91*(A5), 5711–5718. https://doi.org/10.1029/JA091iA05p05711

Lanzerotti, L. J. (2004). Solar and solar radio effects on technologies. In *Solar and space weather radiophysics* (pp. 1–16). Netherlands: Springer. https://doi.org/10.1007/1-4020-2814-8_1

Lanzerotti, L. J., & Baker, D. N. (2017). Space weather research: Earth's radiation belts. *Space Weather*, *15*, 742–745. https://doi.org/10.1002/2017SW001654

Li, W., Thorne, R. M., Ma, Q., Ni, B., Bortnik, J., Baker, D. N., … Claudepierre, S. G. (2014). Radiation belt electron acceleration by chorus waves during the 17 March 2013 storm. *Journal of Geophysical Research: Space Physics*, *119*, 4681–4693. https://doi.org/10.1002/2014JA019945

Li, X., Baker, D. N., Kanekal, S. G., Looper, M., & Temerin, M. (2001). Long term measurements of radiation belts by SAMPEX and their variations. *Geophysical Research Letters*, *28*(20), 3827–3830. https://doi.org/10.1029/2001GL013586

Lohmeyer, W., Carlton, A., Wong, F., Bodeau, M., Kennedy, A., & Cahoy, K. (2015). Response of geostationary communications satellite solid-state power amplifiers to high-energy electron fluence. *Space Weather*, *13*, 298–315. https://doi.org/10.1002/2014SW001147

Miyoshi, Y., Morioka, A., Obara, T., Misawa, H., Nagai, T., & Kasahara, Y. (2003). Rebuilding process of the outer radiation belt during the 3 November 1993 magnetic storm: NOAA and Exos-D observations. *Journal of Geophysical Research*, *108*(A1), 1004. https://doi.org/10.1029/2001JA007542

Morley, S. K., Friedel, R. H. W., Cayton, T. E., & Noveroske, E. (2010). A rapid, global and prolonged electron radiation belt dropout observed with the Global Positioning System constellation. *Geophysical Research Letters*, *37*, L06102. https://doi.org/10.1029/2010GL042772

Morley, S. K., Sullivan, J. P., Henderson, M. G., Blake, J. B., & Baker, D. N. (2016). The Global Positioning System constellation as a space weather monitor: Comparison of electron measurements with Van Allen Probes data. *Space Weather*, *14*, 76–92. https://doi.org/10.1002/2015SW001339

Pierrard, V., & Lopez Rosson, G. (2016). The effects of the big storm events in the first half of 2015 on the radiation belts observed by EPT/PROBA-V. *Annales de Geophysique*, *34*(1), 75–84. https://doi.org/10.5194/angeo-34-75-2016

Reeves, G., Baker, D., Belian, R., Blake, J., Cayton, T., Fennell, J., … Spence, H. (1998). The global response of relativistic radiation belt electrons to the January 1997 magnetic cloud. *Geophysical Research Letters*, *25*(17), 3265–3268. https://doi.org/10.1029/98GL02509

Reeves, G. D. (2007). Radiation Belt Storm Probes: A new mission for space weather forecasting. *Space Weather*, *5*, S11002. https://doi.org/10.1029/2007SW000341

Reeves, G. D., Chen, Y., Cunningham, G. S., Friedel, R. W. H., Henderson, M. G., Jordanova, V. K., … Zaharia, S. (2012). Dynamic Radiation Environment Assimilation Model: DREAM. *Space Weather*, *10*, S03006. https://doi.org/10.1029/2011SW000729

Sarno-Smith, L. K., Larsen, B. A., Skoug, R. M., Liemohn, M. W., Breneman, A., Wygant, J. R., & Thomsen, M. F. (2016). Spacecraft surface charging within geosynchronous orbit observed by the Van Allen Probes. *Space Weather*, *14*, 151–164. https://doi.org/10.1002/2015SW001345

Shprits, Y. Y., Thorne, R. M., Friedel, R., Reeves, G. D., Fennell, J., Baker, D. N., & Kanekal, S. G. (2006). Outward radial diffusion driven by losses at magnetopause. *Journal of Geophysical Research*, *111*, A11214. https://doi.org/10.1029/2006JA011657

Spogli, L., Alfonsi, L., De Franceschi, G., Romano, V., Aquino, M. H. O., & Dodson, A. (2009). Climatology of GPS ionospheric scintillations over high and mid-latitude European regions. *Annales de Geophysique*, *27*(9), 3429–3437. https://doi.org/10.5194/angeo-27-3429-2009

Stratton, J. M., Harvey, R. J., & Heyler, G. A. (2013). Mission overview for the Radiation Belt Storm Probes mission. *Space Science Reviews*, *179*(1-4), 29–57. https://doi.org/10.1007/s11214-012-9933-x

Subbotin, D. A., & Shprits, Y. Y. (2009). Three-dimensional modeling of the radiation belts using the Versatile Electron Radiation Belt (VERB) code. *Space Weather*, *7*, S10001. https://doi.org/10.1029/2008SW000452

Summers, D., Ni, B., & Meredith, N. P. (2007). Timescales for radiation belt electron acceleration and loss due to resonant wave-particle interactions: 2. Evaluation for VLF chorus, ELF hiss, and electromagnetic ion cyclotron waves. *Journal of Geophysical Research*, *112*, A04207. https://doi.org/10.1029/2006JA011993

Svalgaard, L. (2013). Solar activity—Past, present, future. *Journal Space Weather Spac.*, *3*, A24.

Thomsen, M. F., Henderson, M. G., & Jordanova, V. K. (2013). Statistical properties of the surface-charging environment at geosynchronous orbit. *Space Weather*, *11*, 237–244. https://doi.org/10.1002/swe.20049

Thorne, R. M., & Kennel, C. F. (1971). Relativistic electron precipitation during magnetic storm main phase. *Journal of Geophysical Research*, *76*(19), 4446–4453. https://doi.org/10.1029/JA076i019p04446

Thorne, R. M., Li, W., Ni, B., Ma, Q., Bortnik, J., Chen, L., … Kanekal, S. G. (2013). Rapid local acceleration of relativistic radiation belt electrons by magnetospheric chorus. *Nature*, *504*(7480), 411–414. https://doi.org/10.1038/nature12889

Tsyganenko, N. A. (2002), A model of the near magnetosphere with a dawn-dusk asymmetry, 2. Parameterization and fitting to observations, *Journal of Geophysical Research*, *107*(A8), 1176. https://doi.org/10.1029/2001JA000220

Ukhorskiy, A. Y., Mauk, B. H., Fox, N. J., Sibeck, D. G., & Grebowsky, J. M. (2010). Radiation Belt Storm Probes: Resolving fundamental physics with practical consequences. *Journal of Atmospheric and Solar - Terrestrial Physics*, *73*(11-12), 1417–1424. https://doi.org/10.1016/j.jastp.2010.12.005

Wrenn, G. L. (1995). Conclusive evidence for internal dielectric charging anomalies on geosynchronous communications spacecraft. *Journal of Spacecraft and Rockets*, *32*(3), 514–520. https://doi.org/10.2514/3.26645

Zanetti, L. J., Mauk, B. H., Fox, N. J., Barnes, R. J., Weiss, M., Sotirelis, T. S., … Becker, H. N. (2014). The evolving space weather system—Van Allen Probes contribution. *Space Weather*, *12*, 577–581. https://doi.org/10.1002/2014SW001108